PERGAMON

International Journal of Heat and Mass Transfer 41 (1998) 3357–3371

International Journal of HEAT and MASS TRANSFER

A comparative study of radiative heat transfer modelling in gas-fired furnaces using the simple grey gas and the weighted-sum-of-grey-gases models

F. Liu[a,*], H. A. Becker[a], Y. Bindar[b]

[a] *Centre for Advanced Gas Combustion Technology, Department of Chemical Engineering, Queen's University at Kingston, Ontario, Canada K7L 3N6*

[b] *Department of Chemical Engineering, Faculty of Industrial Technology, Institute Technology of Bandung, Bandung 40132, Indonesia*

Received 20 November 1996; in final form 28 February 1998

Abstract

Radiative heat transfer in, (a) two model enclosures containing a high-temperature CO_2–H_2O mixture, and (b) a real multiburner natural-gas-fired furnace, was studied using the simple grey gas model and the more realistic weighted-sum-of-grey-gases model of gas radiative properties. The radiative transfer equation was solved by the discrete-ordinates method. When the radiative transfer equation and the enthalpy transport equation are solved simultaneously, the simple grey gas model yields wall heat flux distributions in reasonably good agreement with those of the weighted-sum-of-grey-gases model but underpredicts gas temperature levels. When the temperature field is specified and the radiative transfer equation is then solved, however, the wall heat flux distributions predicted using the simple grey gas model are in serious error compared to those from the weighted-sum-of-grey-gases model. The weighted-sum-of-grey-gases model predicts more accurate heat flux and gas temperature distributions than the simple grey gas model in the full modelling of the gas-fired furnace.

Nomenclature

$a_{\varepsilon,v}$ weighting factor of the nth grey gas in the fitting of gas emissivity
$a_{\alpha,v}$ weighting factor of the nth grey gas in the fitting of gas absorptivity
D separation distance between parallel walls [m]
I total (spectrally integrated) radiation intensity [W m^{-2} sr^{-1}]
L radiation beam length [m]
p partial pressure [atm]
$\mathbf{q}$ heat flux density vector
S surface area [m^2]
T temperature [K]
V volume [m^3]
x, y, z cartesian coordinates [m].

Greek symbols
α absorptivity
$\delta_{\mathbf{n}}$ unit normal vector of a surface pointing to the gas side
$\delta_{\mathbf{o}}$ unit vector in the direction of radiation propagation
ε total gas emissivity or surface emissivity
κ_e effective absorption coefficient in simple grey gas approximation [m^{-1}]
κ_v absorption coefficient of the vth grey gas component [m^{-1}]
ξ, η, μ direction cosines
σ Stefan–Boltzmann constant, 5.67×10^{-8} [W m^{-2} K^{-4}]
Ω solid angle [sr]
$\nabla\cdot\mathbf{q}$ source term due to radiative transfer [kW m^{-3}].

Subscripts
1, 2 value at walls of the parallel planes enclosure

* Corresponding author. Current address: Combustion Technology, ICPET, National Research Council, M-9, Montreal Road, Ottawa, ON, Canada K1A 0R6. Tel.: 001 613 993 9470; fax: 001 613 957 7869; e-mail: fengshang.liu@nrc.ca

0017–9310/98 $19.00
PII: S0017–9310(98)00098–2

b blackbody
c centerline value in the parallel planes enclosure
g gas
m mean
v vth grey gas
s surface.

Acronyms
DOM discrete-ordinates method
EWB exponential wide-band
LBL line-by-line
RTE radiative transfer equation
SNB statistical narrow-band
SGG simple grey gas
WSGG weighted-sum-of-grey-gases.

1. Introduction

Radiative transfer dominates heat transfer in large-scale, high-temperature systems such as gas-fired furnaces and boilers. Accurate calculation of radiative transfer is then of crucial importance for the prediction of the thermal performance. In addition, radiation significantly affects the gas temperature field and consequently has a strong impact on the predicted formation of pollutants. However, accurate calculation of radiative transfer is very complex, primarily due to the extremely strong spectral dependence of the radiative properties of the combustion products. In natural gas-fired combustion systems, the dominant radiating species are CO_2 and H_2O. The effects of CH_4 and CO are usually highly localised in the near-burner regions and, thus, of minor significance.

Recently, considerable attention has been paid to the development of accurate and efficient methods for handling the spectral structure of the radiative properties of gases. The methods are of two classes. Those of Class 1 treat the absorption coefficient. Most of the solution techniques for the differential radiative transfer equation (RTE) found in the literature, such as the discrete-ordinates method (DOM) and other differential approximate methods, can then be used with only minor adjustments. Class 1 methods include the line-by-line (LBL) method [1, 2], the weighted-sum-of-grey-gases (WSGG) method [3, 4] among others. The LBL method entails the exact treatment of spectral radiative properties. It is extremely computationally intensive and therefore, at present, impractical for engineering calculations; however, it is useful for developing benchmark solutions to validate approximate methods. The WSGG method is computationally much more efficient than LBL. It entails only moderate increase in execution time (about an order of magnitude) compared to the simple grey gas (SGG) model. Therefore, the WSGG is a highly attractive and practical choice to be used in the full modelling of gas-fired combustion systems. It has the limitation that participating surfaces must be treated as grey but for industrial problems this is usually an acceptable, even necessary, simplification. Methods of Class 2 do not model the absorption coefficient; instead, they yield the band transmittance and absorptance for given radiation paths over narrow or wide spectral ranges. These methods are appropriate to solution of the integral form of the RTE. The popular band models include the exponential wide-band (EWB) model [5, 6] and the statistical narrow-band (SNB) model [7, 8]. Band models cannot be easily implemented into the RTE in multidimensions mainly because they require a ray-tracing method to solve the resultant band averaged RTE which contains extra formidable source terms [8].

In the full simulation of combustion systems, the radiative transport equation, traditionally known in radiation physics as 'the equation of transfer', a differentio-integral equation in its full form which includes scatter, must be solved together, as a fully coupled system, with the partial differential equations of materially-mediated transport (as opposed to photon-mediated; specifically, the equations of material, momentum and enthalpy transport). We herein refer to the former as the RTE and to the latter as the MMTE's. In terms of the present focus, the RTE describes the radiative intensity field I whereas the MMTE's govern the temperature field T. Despite rapid progress in computer speed and capacity and in the theory of approximate band parameter estimation [6], the incorporation of the LBL method, the SNB or the EWB model in a genefic computer code for the full simulation of complex, large-scale, strongly three-dimensional combustion systems will remains computationally prohibitive. Therefore, simpler treatments of the radiative properties of furnace gases are practically necessary for such systems. It is worth noting that the state of the art of modelling radiative transfer in such cases it still largely based on the SGG approximation, e.g., Adams and Smith [9] and Soufiani and Djavdan [10]. Computations using the WSGG model have been reported by Soufiani and Djavdan [10] for an axi-symmetrical furnace, with fields effectively two-dimensional. However, their computations using WSGG were decoupled from the calculation of the gas temperature field (the solution of the MMTE's). In their approach, they first estimated gas temperature from a full simulation employing the SGG model. The RTE was then solved again for the radiant intensity field corresponding to this temperature field, using the SNB and WSGG radiative property models, yielding the wall radiative fluxes and heat transfer rates. This exercise is of some interest but falls significantly short of a true full simulation in which the intensity and temperature fields are found together under a single radiation model. Since the full simulation is fairly easily done with the SGG model, and we have also been able to achieve it for complex

furnace problems with the WSGG model, it is of interest to make critical comparisons of predictions with these models under two different scenarios:

(1) Starting with a specified field of gas temperature and composition, solve the RTE for the radiant intensity field. Here the temperature field is given, not computed. The field may be defined experimentally or it may be hypothetical. The object is to compute and compare radiative fluxes by solving the RTE. This scenario lends itself to the generation of benchmark solutions of radiative transfer which can be used for testing and calibration.
(2) Starting with no assumptions about the gas temperature field, solve the full system of equations for the fields of both radiant intensity and gas temperature. Compare predictions with each other and with experimental data. Excellent benchmark solutions are typically lacking.

The object of the present study is thus to investigate the performance of the SGG and WSGG models under both scenarios and, from this, to arrive at an evaluation of their individual and relative merits and limitations in the simulation of industrial furnaces. In the evaluation, we use comparisons with the experimental data of Bindar [11] on a natural-gas-fired multiburner research furnace of semi-industrial scale. The evaluation can thus be regarded as practically valid.

2. Formulation

2.1. Simple grey gas (SGG) model

The simplest treatment of radiative properties of gaseous combustion products is the SGG approximation. This model supposes that radiant absorption and emission by gas molecules are independent of the frequency of the radiation, regardless of the strong dependency on frequency found in reality. Consequently, the radiative properties of a gas mixture are represented by a single parameter, the effective absorption coefficient. Lallemant and Weber [12] give a comprehensive discussion of the grey gas model and the effective absorption coefficient. The advantage of this model are its simplicity and minimal resultant execution times and it therefore has commonly been used in generic CFD programs for modelling radiative transfer.

Under the grey gas assumption, the radiative transfer equation (RTE) for the radiation intensity (integrated over the entire spectrum) in three-dimensional cartesian coordinates is, neglecting scattering of radiation which is negligible in natural-gas-fired combustion systems,

$$\xi\frac{\partial I}{\partial x}+\eta\frac{\partial I}{\partial y}+\mu\frac{\partial I}{\partial z}=-\kappa_e I+\kappa_e I_b. \tag{1}$$

In the full modelling of a gas-fired furnace, the RTE is solved for a 'known' temperature field determined by the MMTE's. The source term for radiative transfer in the enthalpy transport equation (the key MMTE) is

$$-\nabla\cdot\mathbf{q}=\kappa_e\left(\int_{4\pi} I\,\mathrm{d}\Omega-4\sigma T_g^4\right) \tag{2}$$

which represents the rate of radiant heating per unit volume; we herein call this the radiant heating density. When the radiant heating density, rather than the temperature of the gas, is specified (a situation relevant to the full modelling of a combustion system where the gas temperature field is updated by the energy equation), an extra equation, which follows from equation (2), is required to relate the blackbody radiation intensity, $I_b=\sigma T_g^4/\pi$, to $\nabla\cdot\mathbf{q}$:

$$I_b=\frac{1}{4\pi}\left(\int_{4\pi} I\,\mathrm{d}\Omega+\nabla\cdot\mathbf{q}/\kappa_e\right). \tag{3}$$

Consistent with the limitation of the SGG and WSGG models, the bounding surfaces of the system are herein assumed to be grey and diffusely reflecting and emitting, i.e., grey Lambert surfaces. The wall boundary condition for the leaving radiation intensity is then

$$I(\delta_o)=\varepsilon_s I_b(T_s)+\frac{1-\varepsilon_s}{\pi}\int_{2\pi,\delta_n\cdot\delta_o'<0}|\delta_n\cdot\delta_o'|I(\delta_o')\,\mathrm{d}\Omega',\quad \text{for } \delta_n\cdot\delta_o>0. \tag{4}$$

The wall (surface) heat flux density is

$$q_n=\int_{4\pi}\delta_n\cdot\delta_o' I\,\mathrm{d}\Omega=\varepsilon_s(E_s-G_s)=\varepsilon_s\sigma T_s^4+\varepsilon_s\int_{2\pi,\delta_n\cdot\delta_o'<0}\delta_n\cdot\delta_o' I(\delta_o')\,\mathrm{d}\Omega'. \tag{5}$$

An optimal value of the SGG effective absorption coefficient for a given situation can be found by trial and error, by comparing the numerical results obtained using the SGG model with experimental data or with more accurate numerical results based on a more rigorous treatment of gas radiation. The optimal value may be defined as that which gives agreement on the total heat flux to sinks when the gas temperature field is specified. However, it will be found that predictions with the optimal coefficient do not, in general, accurately match the distribution of heat flux density over the sinks, or the temperature distribution over the refractories, or the temperature distribution in the gas. Moreover, the optimal value for any one situation is not generally optimal for another.

The general method for making a realistic best estimate of the effective absorption coefficient from the known properties of emission by the gas is based on interpretation of the total emissivity, ε_g, of the gas upon the bounding surface. The estimate involves use of a mean beam length L_m and a characteristic gas temperature. The

characteristic temperature can be the volume-average gas temperature T_m, in which case

$$\kappa_e = -(1/L_m)\ln[1-\varepsilon_g(T_m, L_m)] \quad (6)$$

or the local temperature, T, giving a locally varying value

$$\kappa_e = -(1/L_m)\ln[1-\varepsilon_g(T, L_m)]. \quad (7)$$

We here estimate the mean beam length, following Hottel and Sarofim [13], as

$$L_m = 0.9L_0 \equiv 3.6V/S \quad (8)$$

where $L_0 = 4V/S$ is the limit value of L_m as $\kappa_e L_m \to 0$.

Adams and Smith [9] used an experimentally determined, axially-varying gas emissivity to estimate the effective absorption coefficient for an axisymmetrical system. In general, the total emissivity of the gas mixture can be calculated using the EWB model, by the polynomial fitting expression of Modak [14], or from the well-known gas emissivity charts [13]. The expressions of Modak and Smith et al. [15], discussed below, were used in the present study to estimate the total emissivity of CO_2/H_2O/clear-gas mixtures. Only CO_2 and H_2O are here considered as radiating species and the total pressure is taken to be $P = 101.3$ kPa. In addition, the partial pressure ratio of CO_2–H_2O is supposed to be 1 : 2, which agrees sufficiently with the mean molecular formula [16], $C_{1.015}H_{3.976}N_{0.011}$, for the natural gas used in our experimental studies. For a CO_2–H_2O mixture of $p_{CO_2} = 0.1P$ and $p_{H_2O} = 0.2P$ (corresponding to natural gas/air combustion of near stoichiometric conditions), these expressions yield similar total emissivities for a wide range of temperature and fairly wide range of mean beam length (see Fig. 5 in Section 3.2). The WSGG model parameters of Smith et al. are applicable for CO_2–H_2O mixtures with the partial pressures that they considered, namely $p_{CO_2} = 0.1P$ and $p_{H_2O} = 0.1P$ or $p_{CO_2} = 0.1P$ and $p_{H_2O} = 0.2P$. The expression of Modak is applicable to mixtures of arbitrary partial pressures, but the total pressure must be one atmosphere. Since the mean or local gas temperatures are in general unknown a priori in the full modelling of a combustion system, the absorption coefficient has to be treated as an eigenvalue.

2.2. Weighted-sum-of-grey-gases (WSGG) model

The WSGG model, introduced by Hottel and co-workers (see Hottel and Sarofim [13]) in the context of the zone method, can be interpreted to express the total emissivity and absorptivity of a conical column of uniform gas of length L, at temperature T_g, exchanging radiation with a grey-Lambert surface element dS at its apex at temperature T_s:

$$\varepsilon_g(T_g, L) = \sum_{v=1}^{N} a_{\varepsilon,v}(T_g)[1-\exp(-\kappa_v L)] \quad (9)$$

$$\alpha_{gs}(T_g, T_s, L) = \sum_{v=1}^{N} a_{\alpha,v}(T_g, T_s)[1-\exp(-\kappa_v L)] \quad (10)$$

where $a_{\varepsilon,v}(T_g)$ and $a_{\alpha,v}(T_g, T_s)$ denote, respectively, the emission and absorption weighting factors for the vth 'grey gas' component. The bracketed quantity is the emissivity of the vth grey gas, with absorption coefficient κ_v and path length L. The coefficient for $v = 1$ is assigned a value of zero and effectively accounts for windows in the spectrum between regions of high absorption. The weighting factors $a_{\varepsilon,v}(T_g)$ and $a_{\alpha,v}(T_g, T_s)$ may be interpreted as the fraction of blackbody energy residing in spectral regions where the absorption coefficient is around κ_v. The weighting factors must be positive and sum to unity,

$$\sum_{v=1}^{N} a_{\varepsilon,v}(T_g) = 1 \quad (11)$$

$$\sum_{v=1}^{N} a_{\alpha,v}(T_g, T_s) = 1. \quad (12)$$

In practice, $a_{\varepsilon,v}(T_g)$, $a_{\alpha,v}(T_g, T_s)$ and κ_v are obtained by fitting equations (9) and (10) to the total emissivity and absorptivity data [13, 15] or using the spectral line-based WSGG procedure of Denison and Webb [4]. Usually, the use of two or three grey gas components and a clear gas ($\kappa_1 = 0$) is sufficient to accurately represent the total emissivity and absorptivity of a CO_2/H_2O/clear-gas mixture over a wide range of temperature and partial-pressure path-length product [13, 15, 17].

For a CO_2/H_2O/clear-gas mixture with $p_{CO_2} = 0.1P$, $p_{H_2O} = 0.2P$, and $P = 101.3$ kPa, weighting factors have been reported by Smith et al. [15] and Truelove [17], among others. Smith et al. employed third order polynomials for both $a_{\varepsilon,v}(T_g)$ and $a_{\alpha,v}(t_g, T_s)$, i.e.,

$$a_{\varepsilon,v} = \sum_{j=1}^{4} b_{\varepsilon,v,j} T_g^{j-1} \quad (13)$$

$$a_{\alpha,v} = \sum_{j=1}^{4} \left(\sum_{k=1}^{4} c_{\alpha,v,j,k} T_s^{k-1} \right) T_g^{j-1}. \quad (14)$$

In contrast, Truelove used simple linear expressions,

$$a_{\varepsilon,v} = b_{v,1} + b_{v,2} T_g, \quad (15)$$

$$a_{\alpha,v} = b_{v,1} + b_{v,2} T_s \quad (16)$$

where the same fitting coefficients are used for both $a_{\varepsilon,v}$ and $a_{\alpha,v}$. Values of WSGG model parameters of Truelove ($b_{v,1}$, $b_{v,2}$, and κ_v) are also available in Rhine and Tucker [18]. Effects of using the complex WSGG expression of Smith et al. and the simple expression of Truelove on the prediction of radiative transfer are examined in next section.

The RTE for the vth 'grey gas' component of the radiating gas mixture is

$$\xi \frac{\partial I_v}{\partial x} + \eta \frac{\partial I_v}{\partial y} + \mu \frac{\partial I_v}{\partial z} = \kappa_v [a_{\varepsilon,v}(T) I_b(T) - L_v]. \quad (17)$$

The total intensity (integrated over the entire spectrum) is simply

$$I = \sum_{v=1}^{N} I_v \tag{18}$$

and heat flux components are calculated as

$$q_i = \int_{4\pi} \delta_{\mathbf{i}} \cdot \delta_{\mathbf{o}} I \, \mathrm{d}\Omega = \sum_{v} \int_{4\pi} \delta_{\mathbf{i}} \cdot \delta_{\mathbf{o}} I_v \, \mathrm{d}\Omega, \quad i = x, y, \text{or } z. \tag{19}$$

When the field of the radiant heating density, instead of temperature, is specified, the RTEs must be solved simultaneously with the following equation to update the medium temperature (where $\nabla \cdot \mathbf{q}$ is known):

$$T = \left[\left(\nabla \cdot \mathbf{q} + \sum_{v=1}^{N} \int_{4\pi} \kappa_v I_v \, \mathrm{d}\Omega \right) \Big/ 4\sigma \sum_{v=1}^{N} \kappa_v a_{\varepsilon,v} \right]^{1/4}. \tag{20}$$

The boundary condition for the leaving intensity at a grey Lambert surface, similar to equation (4), can be approximated as [4, 10]

$$I_v(\delta_o) = \varepsilon_s a_{\varepsilon,v}(T_s) I_b(T_s) + \frac{1-\varepsilon_s}{\pi} \int_{2\pi, \delta_{\mathbf{n}} \cdot \delta'_{\mathbf{o}} < 0} |\delta_{\mathbf{n}} \cdot \delta'_{\mathbf{o}}| I_v(\delta'_{\mathbf{o}}) \, \mathrm{d}\Omega', \quad \text{for } \delta_{\mathbf{n}} \cdot \delta_{\mathbf{o}} > 0. \tag{21}$$

For easy identification, this is hereinafter called the conventional boundary condition. A more rigorous treatment proposed by Becker [19] gives

$$I_v(\delta_o) = \varepsilon_s a_{\alpha,v}(T_s, T_m) I_b(T_s) + \frac{I-\varepsilon_s}{\pi} \int_{2\pi, \delta_{\mathbf{n}} \cdot \delta'_{\mathbf{o}} < 0} |\delta_{\mathbf{n}} \cdot \delta'_{\mathbf{o}}| I_v(\delta'_{\mathbf{o}}) \, \mathrm{d}\Omega', \quad \text{for } \delta_{\mathbf{n}} \cdot \delta_{\mathbf{o}} > 0. \tag{22}$$

The radiant heating energy is now calculated as

$$-\nabla \cdot \mathbf{q} = \sum_{v=1}^{N} \int_{4\pi} \kappa_v I_v \, \mathrm{d}\Omega - 4 \left(\sum_{v=1}^{N} \kappa_v a_{\varepsilon,v} \right) \sigma T^4. \tag{23}$$

3. Results and discussion

The radiative transfer equation was solved using DOM [20]. In the two model problems examined below, spatial differencing was done by the positive scheme [21] in which the weighting factor of spatial differencing varies between 0.5 and unity in terms of the local conditions to ensure the positivity of radiation intensity. It is equivalent to the hybrid differencing scheme in CFD. The diamond scheme [21], equivalent to the central differencing scheme in CFD, was used in modelling the gas-fired furnace. The T_6 quadrature set [22] was employed in all the calculations.

3.1. Parallel planes enclosure with specified gas temperature field

3.1.1. The situation

Consider an H_2O–CO_2 gas mixture at 101.3 kPa between two parallel, infinite, grey and diffuse walls, a distance D apart, at equal temperatures T_1 and T_2. A parabolic gas temperature profile between the two walls is supposed, i.e. $T_g = T_s - 4(T_s - T_c)x/D + 4(T_s - T_c)x^2/D^2$. The partial pressures of H_2O and CO_2 are $p_{H_2O} = 2/3P$ and $p_{CO_2} = 1/3P$ (corresponding to stoichiometric natural-gas/oxygen combustion) and the surface emissivities are $\varepsilon_1 = \varepsilon_2 = 0.8$. The WSGG model constants are taken from Soufiani and Djavdan [10]. The calculation domain was divided into 50 uniform layers. It has been checked that further refinement of the grid does not alter the results. Two sets of calculations were done. The first is for cold walls but hot gas ($T_1 = T_2 = 500$ K, $T_c = 2500$ K), and the second is for hot walls but cold gas ($T_1 = T_2 = 2500$ K, $T_c = 500$ K). This problem was previously investigated by Soufiani and Djavdan [10] using the WSGG and the SNB models. The objectives of calculations in this geometry here are to investigate the behaviour of the SGG model relative to the WSGG model and also to compare the present WSGG results to those of Soufiani and Djavdan.

3.1.2. Results employing a predicted absorption coefficient in the SGG model

The mean beam length is $L_m = 3.6$ V/S $= 1.8D$. The effective absorption coefficient was estimated using the volume averaged temperature, equation (6), with the total gas emissivity estimated using the expression of Modak [14]. The effect of using the local temperature instead of the volume averaged one in the evaluation of the κ_e on the prediction of radiative transfer was not explored for these thermal conditions (it was examined for different thermal conditions, see Section 3.1.4) since the polynomial fitting expression of Modak is good only for temperatures below 2000 K. The conventional boundary condition, equation (21), was used in the WSGG calculations.

Figure 1 shows the variation of wall heat flux density with distance between the walls, Fig. 1(a) and (b). The present WSGG results agree very closely with those of Soufiani and Djavdan [10]. The results of the SGG model differ significantly from those of the WSGG model (by a factor of 3–4), especially for the case of hot wall but cold gas, Fig. 1(b). In addition, the discrepancy between the results of the two models increases with increasing distance between the walls. These observations are consistent with the differences between the results of the WSGG and SNB models demonstrated by Soufiani and Djavdan [10], if we view the SGG, WSGG, and SNB models as a hierarchy of increasing accuracy.

Figure 1 also shows the distribution of $\nabla \cdot \mathbf{q}$ for $D = 1$ m, Fig. 1(c) and (d). For the case of hot gas but cold walls, Fig. 1(c), the results of the WSGG and the SGG models differ significantly around the middle of the enclosure. For the case of hot walls and cold gas, Fig. 1(d), they differ considerably nearly everywhere, except close to the walls.

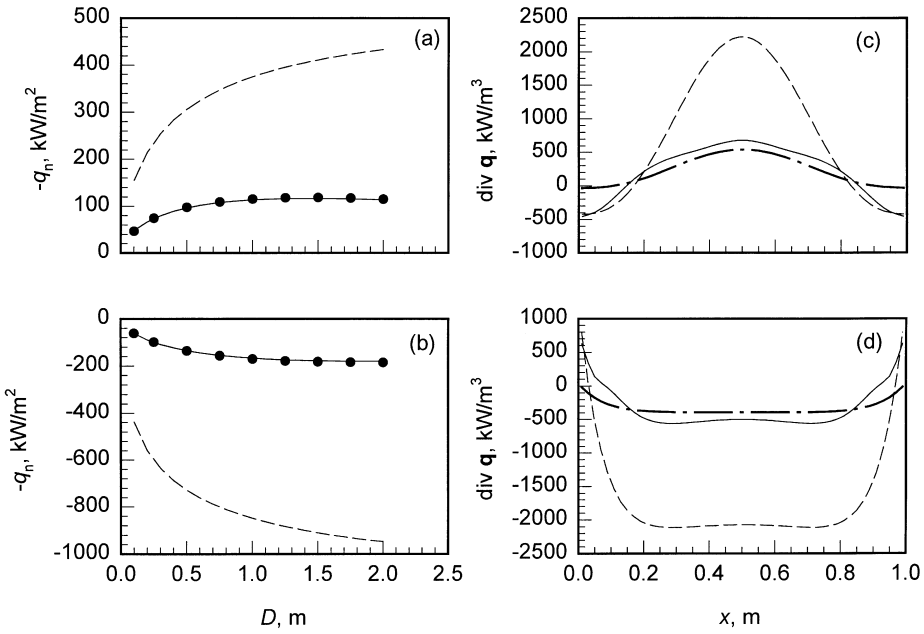

Fig. 1. Comparison of wall heat flux densities and radiant heating densities in a parallel-plane enclosure, using the SGG and WSGG models: (a) and (c) hot gas, cold walls, and (b) and (d) cold gas, hot walls. Key: solid line, WSGG; dashed line, SGG; symbols, WSGG results of Soufiani and Djavdan [10]; dash–dotted line, SGG with optimised κ_e.

3.1.3. Results employing the optimal absorption coefficient in the SGG model

As discussed in Section 2.1, an optimised value of the effective absorption coefficient for a given problem can be found by trial and error by matching the total heat flux (heat flux summed over all surfaces of the enclosure) predicted by the SGG model to a benchmark value. It is of interest to examine the optimised values of the effective absorption coefficient by employing the results of the WSGG model as the benchmark solution. Figure 2 compares the optimised absorption coefficients with those calculated from equation (6) for both the cold wall and hot wall cases. The effective coefficients based on equation (6) are much higher than the optimised ones, especially for the hot wall case (by an order of magnitude), Fig. 2(b). To directly quantify the difference, the ratios of the calculated κ_es to the optimised ones for four values of D are given in Table 1. The ratio in the cold wall case is much lower than that in the hot wall case; however, it increases more rapidly with increasing D. This is as expected to some extent from the results shown in Fig. 1(a) and (b). The distribution of $\nabla\cdot\mathbf{q}$ predicted using the optimised coefficient for $D = 1$ m is also shown in Fig. 1(c) and (d). The SGG results based on the optimised absorption coefficient are in good agreement with those of the WSGG model, except in regions near the walls, but significantly flattened.

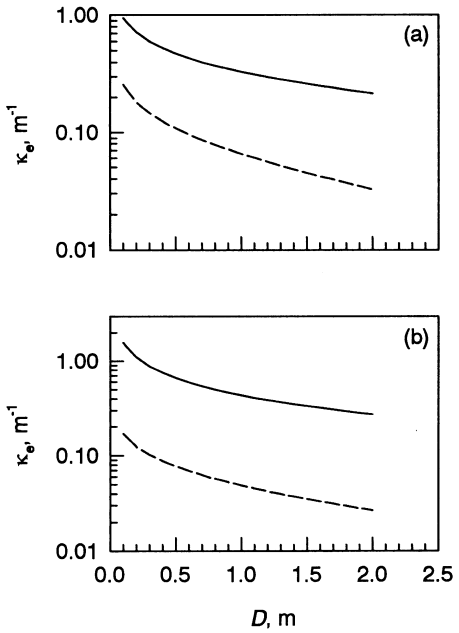

Fig. 2. Comparison of the predicted and optimised κ_e for gas in a parallel-plane enclosure with different separation distances between parallel walls: (a) cold walls, hot gas and (b) hot walls, cold gas. Key: solid line, predicted; dashed line, optimised.

Table 1
Ratio of the predicted absorption coefficient to the optimised one for four separation distances between the walls (optical dimension is based on the predicted κ_e)

Wall	D [m]	Ratio	Opt. dimension
Cold	0.01	2.537	0.036
	0.1	3.693	0.170
	1	5.035	0.594
	2	6.618	0.778
Hot	0.01	8.758	0.074
	0.1	9.196	0.281
	1	8.879	0.783
	2	10.206	0.981

3.1.4. SGG results employing a predicted absorption coefficient based on the local gas temperature

The effect of using the local gas temperature in the calculation of κ_e in the SGG model was investigated under thermal conditions similar to those described in Section 3.1.1 except that for cold wall hot gas case $T_c = 2000$ K and for hot wall cold gas case $T_1 = T_2 = 2000$ K, for the reason given in Section 3.1.2. The predicted wall heat flux densities for different D based on the SGG model employing both the averaged temperature and the local temperature in the evaluation of κ_e are compared in Fig. 3, along with the WSGG results. Even in the existence of a fairly large temperature gradient, the SGG results are only moderately sensitive to how κ_e is calculated; the results are within 20% of each other. It is also interesting that use of the local temperature in the calculation of κ_e yields better results in the cold wall hot gas case, Fig. 3(a), but worse results in the hot wall cold gas case, Fig. 3(b). This can be attributed to the better estimation of the effective coefficient around the middle of the enclosure when using the local gas temperature since use of the averaged temperature results in higher effective coefficients in this region for the cold wall hot gas case, Fig. 5.

3.1.5. Factors affecting the difference between the predicted and the optimised absorption coefficients

As shown in Table 1 and Fig. 2, one factor that affects the difference between the predicted and the optimised absorption coefficients is the separation distance between walls, which is directly related to the mean beam length. Numerical calculations were also conducted to examine the effects of partial pressures of the radiating gases and of the temperature field. In the calculations, the wall conditions were fixed: $T_1 = T_2 = 500$ K, $\varepsilon_1 = \varepsilon_2 = 0.8$ and $D = 1$ m. The results are summarised in Tables 2 and 3. The WSGG model parameters of Smith et al. [15] were used to obtain the benchmark wall heat fluxes for Table 3.

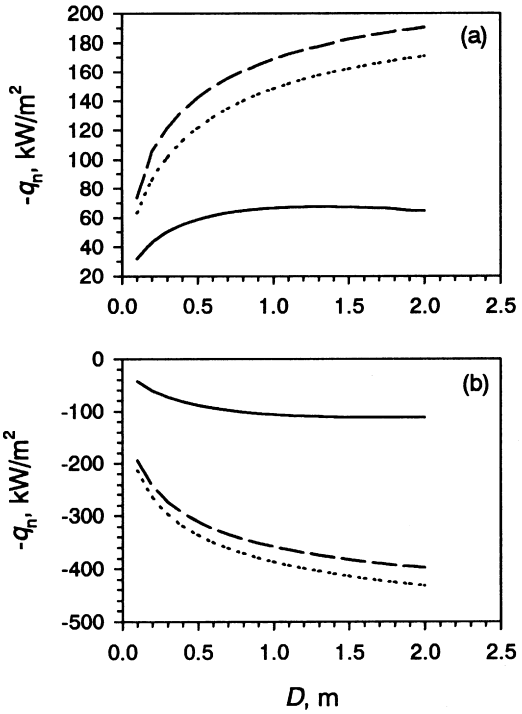

Fig. 3. Comparison of wall heat flux densities in a parallel-plane enclosure with different separation distances: (a) cold walls, hot gas, and (b) hot walls, cold gas. Key: solid line, WSGG; dashed line, SGG using κ_e based on mean gas temperature; dotted line, SGG using κ_e based on local gas temperature.

These results indicate that both the gas temperature distribution and the partial pressures of radiating gases strongly affect the difference between the predicted and the optimised absorption coefficients. The predicted coefficient is always greater than the optimised one. A stronger temperature gradient leads to a larger difference between the predicted and the optimised coefficients. In addition, the difference decreases with decreasing mean gas temperature level. A comparison between results in Tables 2 and 3 shows that the difference decreases with decreasing partial pressures of the radiating gases. These results imply that the SGG model may predict reasonable radiative wall heat fluxes under the conditions of nearly uniform temperature field, low wall temperature, intermediate to large mean beam length, and low partial pressures of radiating gases. These conditions are approximately met in industrial natural-gas-fired furnaces. The performance of the SGG model under these conditions is seen in the next two sections.

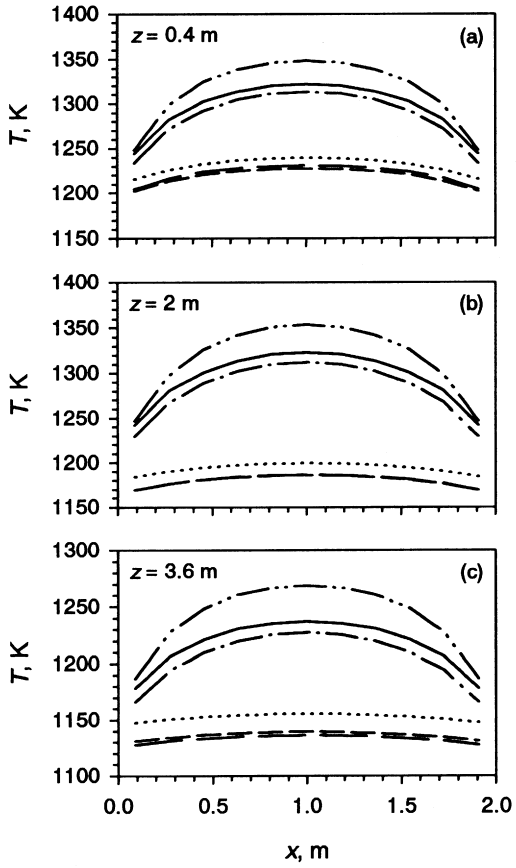

Fig. 4. Comparison of gas temperature distributions in the rectangular enclosure at three locations along the length: (a) $z = 0.4$ m, $y = 1$ m, (b) $z = 2$ m, $y = 1$ m, (c) $z = 3.6$ m, $y = 1$ m. Key: solid line, WSGG using the parameters of Smith et al. [15] and the boundary condition of Becker [19]; dash–dot line, WSGG using the parameters of Smith et al. [15] and the conventional boundary condition; dash–dot–dot line, WSGG using the parameters of Truelove [17] and the conventional boundary condition; short dashed line, SGG with κ_e estimated using mean gas temperature and Smith et al.'s [15] expression for gas emissivity; long dashed line, SGG with κ_e estimated using local gas temperature and Smith et al.'s expression for gas emissivity; dotted line, SGG with κ_e estimated using mean gas temperature and Modak's expression [14] for gas emissivity.

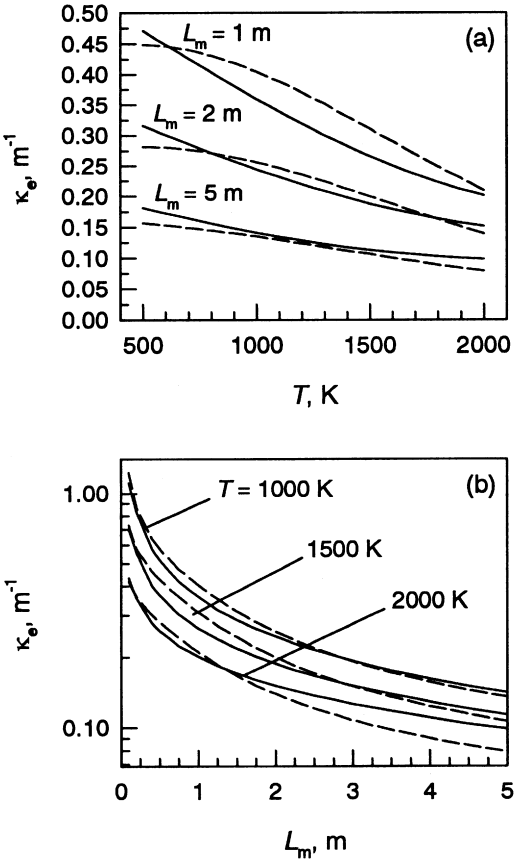

Fig. 5. Variation of the SGG effective absorption coefficient with, (a) temperature, and (b) mean beam length, for an isothermal and homogeneous CO_2–H_2O mixture of $p_{CO_2} = 0.1P$, $p_{H_2O} = 0.2P$, and $P = 101.3$ kPa. Key: solid line, gas emissivity based on the expression of Modak [14]; dashed line, gas emissivity based on the expression of Smith et al. [15].

3.2. Rectangular enclosure with specified fields of radiant heating density or gas temperature

The second test case poses a $2 \times 2 \times 4$ m rectangular enclosure. The boundary conditions of this test case are summarised in Table 4.

The gas in the enclosure is supposed to be homogeneous with $p_{CO_2} = 0.1P$, $p_{H_2O} = 0.2P$, and $P = 101.3$ kPa. All the calculations were done using $11 \times 11 \times 21 = 2541$ uniform control volumes. Further refinement of the grid has negligible effects on the results. It should be pointed out that use of the local temperature in the evaluation of the weighting factors in equation (20) for WSGG calculation with specified $\nabla \cdot \mathbf{q}$ gives rise to non-convergence in the calculation of the temperature field. This may be attributed to the monotonic variation of $\Sigma_v \kappa_v a_{e,v}$ with temperature T. Results of the WSGG model reported here were obtained using the volume averaged temperature in the calculation of the weighting factors in equations (17) and (20). Iteration was stopped when the maximum relative error of the irradiance (incident radiant flux density) is less than 1×10^{-4}.

Two scenarios were investigated. In the first, a uniformly distributed radiant heating density $-\nabla \cdot \mathbf{q} = -5 \times 10^4$ W m^{-3} is specified, and the predicted gas temperature and wall heat flux using the WSGG and SGG models are compared:

(1) The predicted gas temperature distributions are

Table 2
Comparison between the predicted and the optimised absorption coefficients for $p_{CO_2} = 1/3P, p_{H_2O} = 2/3P$, and $P = 101.3$ kPa

Gas temperature distribution	Predicted κ_e [m^{-1}]	Optimised κ_e [m^{-1}]	Ratio
Parabolic $T_c = 2500$ K $T_m = 1834$ K	0.330	0.0655	5.036
Uniform $T = 1834$ K	0.330	0.142	2.316
Parabolic $T_c = 2000$ K $T_m = 1500$ K	0.371	0.0963	3.850
Uniform $T = 1500$ K	0.371	0.211	1.760

Table 3
Comparison between the predicted and the optimised absorption coefficients for $p_{CO_2} = 0.1P$, $p_{H_2O} = 0.2P$, and $P = 101.3$ kPa

Gas temperature distribution	Predicted κ_e [m^{-1}]	Optimised κ_e [m^{-1}]	Ratio
Parabolic $T_c = 2500$ K $T_m = 1834$ K	0.169	0.0523	3.233
Uniform $T = 1834$ K	0.169	1.613	
Parabolic $T_c = 2000$ K $T_m = 1500$ K	0.198	0.0803	2.470
Uniform $T = 1500$ K	0.198	0.155	1.279

Table 4
Boundary conditions of the rectangular enclosure

Wall(s)	Position	T [K]	ε
2×2 m	$z = 0$	1200	0.85
2×2 m	$z = 4$ m	400	0.70
2×4 m	$x = 0$, $x = 2$ m, $y = 0$, $y = 2$ m	900	0.70

shown in Fig. 4. The SGG model underpredicts the temperature levels by as much as 10% relative to the WSGG, Fig. 4(a) and (b). Furthermore, it gives a much flattened distribution.

(2) The SGG results with κ_e estimated from the WSGG expressions of Smith et al. [15] differ only slightly from those obtained with κ_e based on the polynomial fitting expression of Modak [14], because the κ_es are in close agreement under the conditions of this case, Fig. 5. Use of the local gas temperature instead of the volume averaged one in the estimation of κ_e has almost no effects on the predicted temperatures due to the relatively small temperature gradients. Figure 5 shows the variation of κ_e with gas temperatures and the mean beam length over broad ranges of these variables. For this problem, the mean beam length is 1.36 m and the gas temperature varies slightly around 1200 K. Under these conditions, the variation of κ_e with gas temperature is small.

(3) Employing the model parameters of Smith et al. [15], the WSGG predictions of gas temperatures with the boundary condition of Becker [19], equation (22), differ insignificantly, Fig. 4, from those using the conventional boundary condition. The temperatures predicted using the simple linear WSGG weighting factors of Truelove [17] are only about 3% higher than those obtained with Smith, et al.'s third-order expressions [15].

(4) Figure 6 shows the predicted heat flux density distributions at the hot wall ($z = 0$) and the cold wall ($z = 4$ m) along $y = 1$ m, Fig. 6(a) and (b). At the hot wall, Fig. 6(a), using Becker's boundary condition, the WSGG results based on the parameters of Truelove are identical to those based on the parameters of Smith et al. At both walls, the predictions of the WSGG and SGG models differ only slightly from each other. This is not wholly unexpected, based on the consideration that energy conservation here requires that the rate of heat removal through the walls must equal the rate of heat production in the gas. Again, the SGG model gives relatively flattened distributions of heat flux density.

In the second scenario, the temperature field calculated from the WSGG model using the parameters of Smith et al. [15] and the boundary condition of Becker [19] is specified and radiative transfer is calculated using the WSGG (employing different model parameters or boundary condition) and SGG models. The resultant wall heat flux densities are compared in Fig. 6(c) and (d). Similar to what has been found in the one-dimensional case, Fig. 1(a), the SGG model overpredicts the heat flux when the temperature field is specified. The predicted heat flux densities are sensitive to the radiative property model used (SGG or WSGG) but weakly dependent on different forms of boundary condition or model

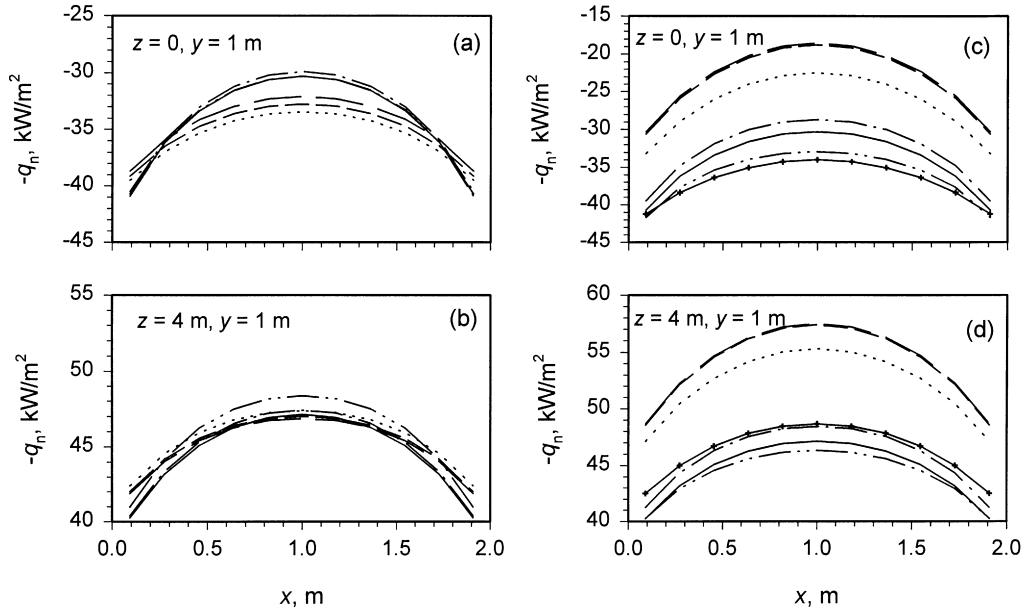

Fig. 6. Comparison of the predicted wall heat flux density distributions in the rectangular enclosure with specified radiant heating density, (a) and (b), and gas temperature field, (c) and (d). Key: solid line with +, SGG using optimised κ_e. For other curves, see Fig. 4.

parameters. Also shown in Fig. 6(c) and (d) are the SGG results based on the optimised absorption coefficient. The optimised SGG heat flux densities are slightly lower than the WSGG results at the hot wall, Fig. 6(c), but slightly higher at the cold wall, Fig. 6(d) indicating flattened distributions of heat flux density. In this case the effective absorption coefficient calculated from the procedure of Smith et al. [15], $\kappa_e = 0.288\ m^{-1}$, is not much higher than the optimised value, $0.169\ m^{-1}$, for reasons discussed in Section 3.1.5.

3.3. Multiburner gas-fired research furnace with experimental data

In the third test case, the effects of using the SGG and the WSGG radiative property models in the full modelling of a multiburner natural gas-fired furnace were investigated by comparing the predicted gas temperature and wall heat flux distributions with experimental data.

The CAGCT research furnace was described in detail elsewhere [11, 16]. The combustion chamber, Fig. 7, is 4.5 m long (y direction), 3 m wide (x direction), and 1 m high (z direction). Three long-flame industrial burners are fitted on the $x = 0$ side-wall at $(x, y, z) = (0, 0.75, 0.5)$, $(0, 1.75, 0.5)$ and $(0, 2.75, 0.5)$ m. The gas exhaust is through an uniform array of holes in the $y = 4.5$ m wall which is made of brick. The furnace floor, $z = 0$, consists of 34 water-cooled panels instrumented to measure the cooling water flow rate and temperature rise, giving the heat flux to each panel. The three other walls and the roof are insulated with 305 mm thick ceramic fiber block refractory. Forty-four thermocouples are embedded at the surface of the refractory to measure local surface temperatures. There are thirty-four probe access ports (seventeen in the roof) which allow the insertion of a traversable thermocouple probe to measure the gas temperature distribution. It has been shown that the dominant mode of heat transfer in this furnace is radiation [11].

The full modelling of the furnace was performed using a three-dimensional finite-volume code [11]. Since the present paper is focused on radiative transfer modelling using the SGG and WSGG radiative property models, the preburn combustion model [23] was used in the calculations in order to reduce the computing time to acceptable levels. In the preburn model, it is supposed that fuel and air are fully reacted at burner exit (furnace inlet), and the combustion products enter the furnace in adiabatic equilibrium. The immediate advantage of this approach is that fully detailed modelling of the nearfield is rendered unnecessary. The burner exit can be represented by a small array of contiguous control volume surface elements.

Numerical calculations were performed for two sets of thermal boundary condition at the furnace floor. In the first set (Run 3 in ref. [11]), all the water-cooled panels of the furnace floor were bare. In the second (Run 5B in ref. [11]), the floor between $y = 0$ and $y = 2.5$ m was

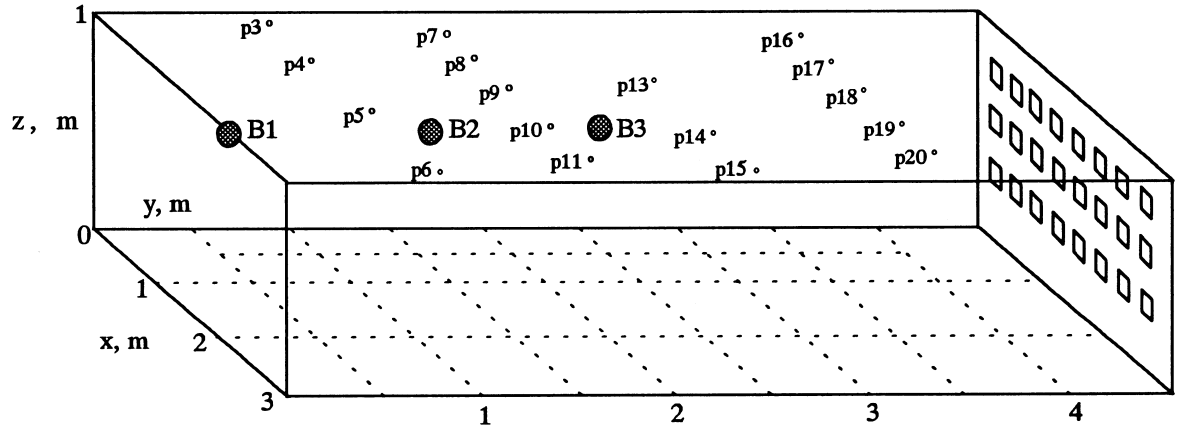

Fig. 7. A schematic of the CAGCT research furnace.

covered with 25 mm thick fiber refractory blanket. All other conditions were the same. The temperature at the surface of water-cooled panels was supposed to be fixed at 70°C. The conduction heat transfer boundary conditions described in detail by Bindar [11] were used at refractory walls. The emissivities of the refractory walls and the water-cooled panels are approximately 0.6 and 0.85, respectively. Further details of these two runs are available in ref. [11].

In the SGG calculations, the effective absorption coefficient is treated as a solution variable and updated using equation (6) (using the mean gas temperature) together with the expression of Modak [14], since it has been demonstrated in the above two model problems that the SGG results are insensitive to the characteristic temperature in the calculation of κ_e or the method for obtaining the total gas emissivity. In the WSGG calculations, three grey gases plus one clear gas were used. Both the complex polynomial expressions for the weighting factors of Smith et al. [15] and the linear expressions of Truelove [17] were employed in the DOM/WSGG calculations, to determine their effects on the predictions. In the WSGG calculation using the model parameters of Smith et al., the boundary condition of Becker [19] was employed to update the radiation intensity at surfaces.

All numerical results presented below were obtained using $30 \times 45 \times 11 = 14\,850$ uniform control volumes. Each burner exit was represented by a 3×3 cluster of control surface elements. The momentum, mass and enthalpy fluxes from each burner were set to match the experimental values. Grid dependence study shows that the results did not fully achieve grid independence. However, it has been checked that further refinement of the grids does not affect the qualitative conclusions of this study but greatly increases the computing time [11].

The computed local heat fluxes on the sink panels using the SGG and WSGG models for Run 3 and Run 5B are compared with the experimental data in Fig. 8. These figures indicate that all the predicted results are in close agreement in both the trend and values with the data, with some deviation of the SGG results from those of the WSGG. Again, the WSGG results based on the model parameters of Truelove [17] differ only slightly from the results obtained using the parameters of Smith et al. [15]. The interesting observation here is that the SGG model predicts sink heat flux distributions in good agreement with those of the WSGG model, as anticipated to some extent from the second test case alone. The predicted refractory wall temperatures are compared with the measured data in Fig. 9. The results based on the two radiative property models are in good agreement with the experimental data, especially for Run 5B.

Comparisons between the predicted gas temperatures and the experimental data are made in Figs 10 and 11 for Run 3 and Run 5B, respectively. The agreement is in general good. The SGG model yields gas temperatures generally lower than the WSGG model and the measurement, similar to what is observed in the second test case, Fig. 4. The WSGG results based on the model parameters of Truelove [17] are in general slightly higher than those based on the model parameters of Smith et al. [15], again as seen in the second test case, Fig. 4. For Run 5B, use of the WSGG model yields more realistic gas temperature distributions than the SGG model at some locations (P15, P16, P19, and P20 in Fig. 11).

Assuming that the temperature field and the total heat loss from the surfaces of the furnace chamber predicted from the full furnace modelling using the WSGG model (employing the model parameters of Smith et al. [15] and the boundary condition of Becker [19]) are the benchmark values, an optimised absorption coefficient in the SGG model was found by matching the total loss from the SGG model to that based on the WSGG model, with the specification of the benchmark temperature field. The

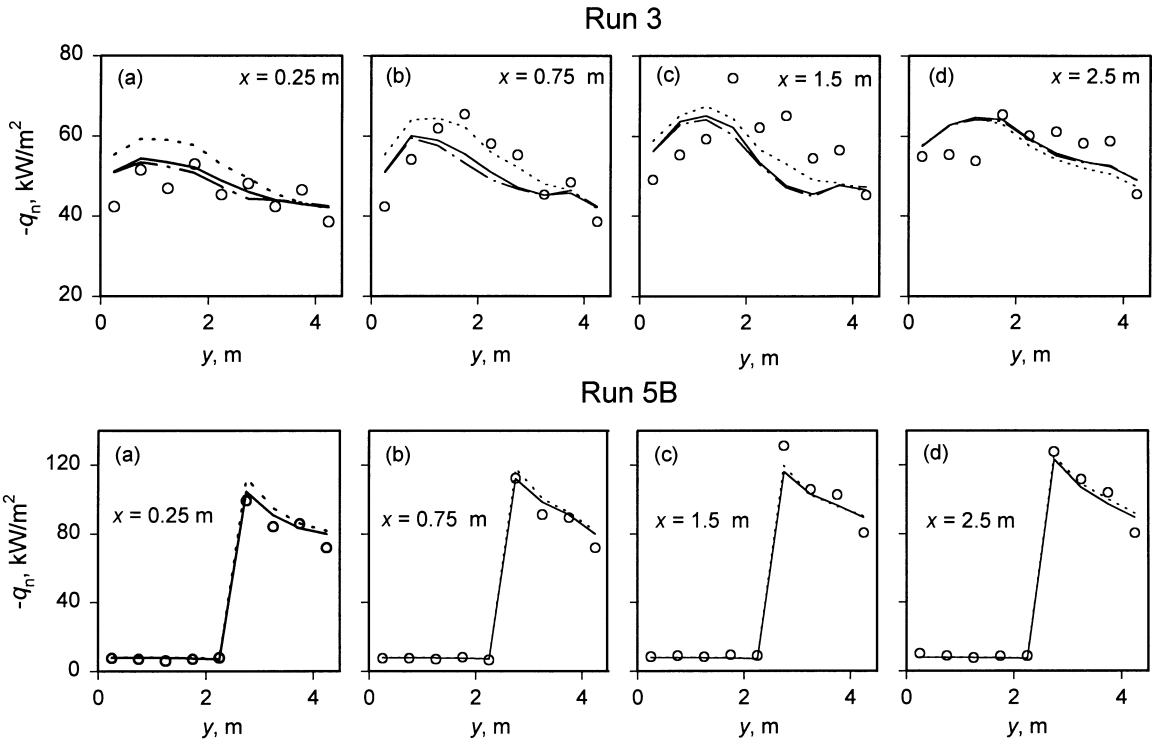

Fig. 8. Comparison between the predicted and the measured wall heat flux density distributions on the floor of the CAGCT furnace at four locations along y direction for Run 3 and Run 5B. Key: circle, measured; solid line, WSGG using the model parameters of Smith et al. [15]; dash–dot line, WSGG using the model parameters of Truelove [17]; dotted line, SGG with predicted κ_e.

mean beam length of this furnace is 1.16 m. Calculations of the optimised absorption coefficient were conducted for three runs, Run 3, Run 5B and Run L. In Run L, the furnace floor between $y = 0$ and $y = 4$ m was covered with 25 mm thick fiber refractory blanket. The purpose of these calculations is to examine the variation of the optimised absorption coefficient with heat transfer boundary conditions. The results of these runs are given in Table 5. It is interesting that the ratio of the predicted absorption coefficient to the optimised one is not significantly different from 1.5 for all three runs. This may suggest that the rule of thumb of obtaining a good estimate of the effective absorption coefficient of the SGG model for large-scale gas-fired furnaces is to divide the predicted one, based on equation (6), by a factor of 1.5.

It has been checked that the SGG model with the optimised absorption coefficient in the full furnace modelling reproduces the correct volume averaged gas temperature and total heat flux to sinks, compared with the results of the full furnace modelling using the WSGG model (the 'benchmark solution').

4. Conclusions

A comparative study has been conducted for radiative transfer modelling using the SGG and WSGG radiative property models in two model problems and a real multiburner, natural-gas-fired research furnace of semi-industrial scale. The effective absorption coefficient in the SGG model can be estimated from the total gas emissivity of the radiating system or found by optimising the SGG results against a benchmark solution. The SGG results are practically insensitive to some alternations: (a) use of the volume averaged temperature or the local temperature, and (b) use of the method to estimate the total gas emissivity in the calculation of κ_e. The estimated absorption coefficient is always higher than the optimised one, reflecting the fact that SGG always overpredicts wall heat flux densities for a specified temperature field. Factors affecting the goodness of the estimated absorption coefficient include the mean beam length, the uniformity and level of the gas temperature field, and the partial pressures of radiating gases. The estimated absorption coefficient significantly deviates from the optimised one under the conditions of high partial pressures of CO_2 and H_2O and strong temperature gradients in the temperature field. Under conditions typical in industrial natural-gas-fired furnaces, the estimated absorption coefficient is about 50% higher than the optimised one. For a given temperature field, the SGG model using the optimised absorption coefficient predicts wall heat flux

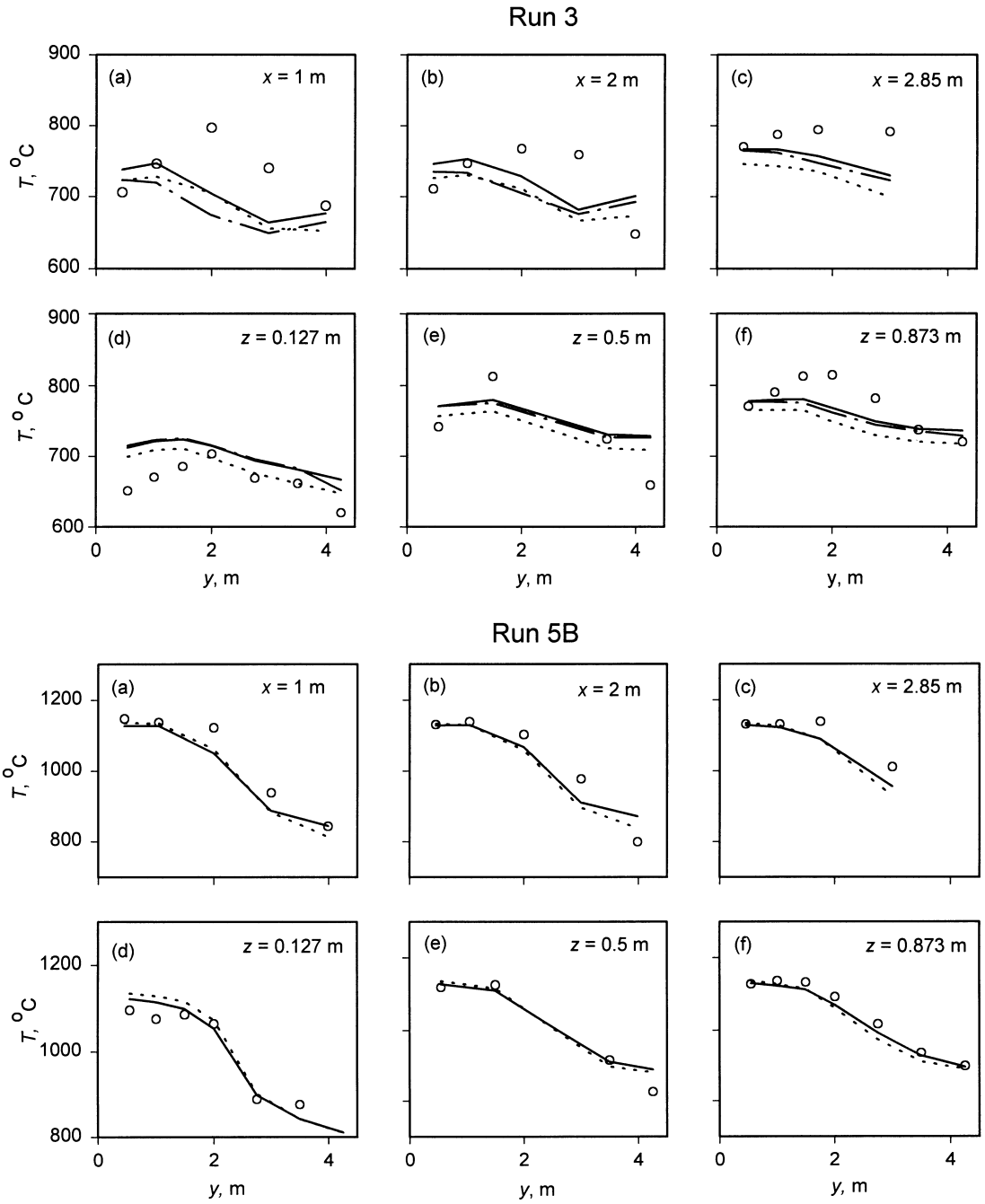

Fig. 9. Comparison between predicted and measured refractory wall temperatures in the CAGCT furnace at selected locations for Run 3 and Run 5B: (a)–(c) roof, (d)–(f) $x = 3.0$ m side wall. Key: see Fig. 8.

densities in good agreement with WSGG model, but flattened. Unfortunately, there is no general rule to obtain the optimised absorption coefficient. Numerical results also show that the predicted wall heat fluxes from the two radiative property models are in reasonably good agreement with each other and with the experimental data in the full furnace modelling or under the condition of specified radiant heating density. However, the SGG model predicts lower gas temperature levels in the full furnace modelling or when the radiant heating density is

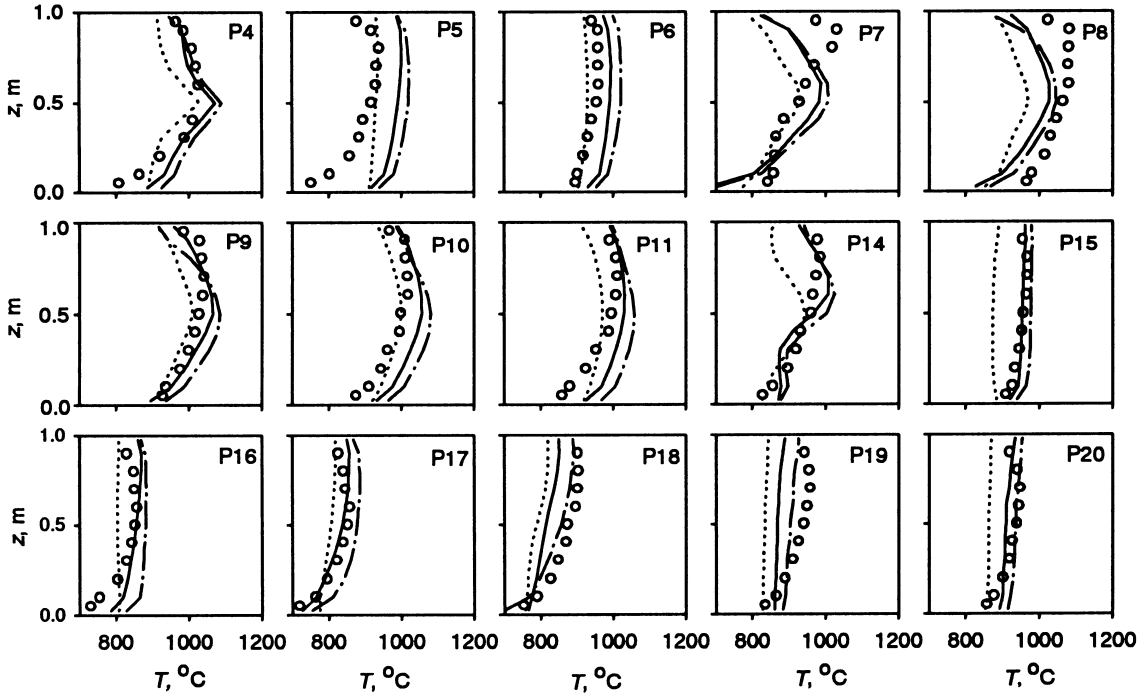

Fig. 10. Comparison between predicted and measured gas temperature distributions over the height of the CAGCT furnace for Run 3. Key: see Fig. 8.

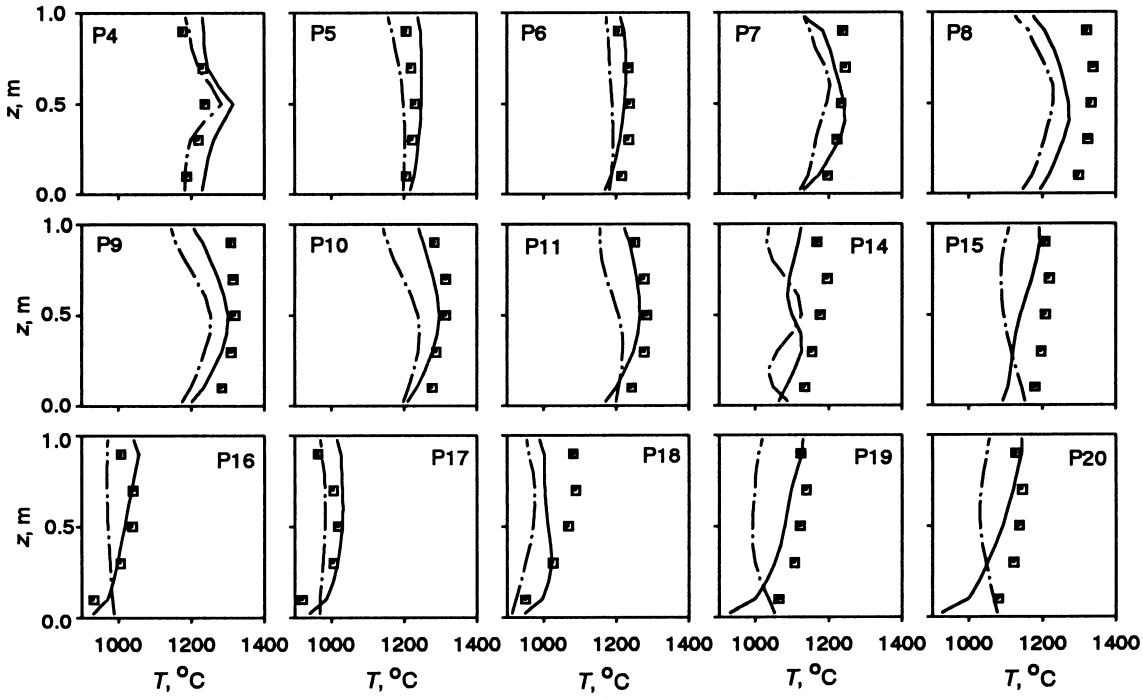

Fig. 11. Comparison between predicted and measured gas temperature distributions over the height of the CAGCT furnace for Run 5B. Key: circle, measured; solid line, WSGG using the model parameters of Smith et al. [15], dash–dot line, SGG using predicted κ_e.

Table 5
Comparison of the predicted and the optimised absorption coefficients from the modelling of the CAGCT research furnace for three heat transfer boundary conditions

	Run 3 (fully open floor)	Run 5B (56% floor covered)	Run L (89% floor covered)
T_m [K]	1195.5	1293.1	1634.2
Predicted κ_e [m^{-1}]	0.296	0.280	0.229
Optimised κ_e [m^{-1}]	0.197	0.199	0.158
Ratio	1.503	1.407	1.449

given. In the WSGG calculations, the results based on the boundary condition of Becker differ only slightly from those based on the conventional boundary condition. The use of different WSGG model parameters has little effect on the predictions. In the full furnace modelling, the WSGG model predicts gas temperature, wall temperature, and wall heat flux in better agreement with experiment than the SGG model. The WSGG model is recommended in the modelling of large-scale gas-fired combustion systems based on the considerations of execution time and accuracy.

Acknowledgements

The authors gratefully acknowledge the funding by the Supply and Service Canada (for the CANMET division of the National Resources Canada); by British Gas plc; and by the National Science and Engineering Research Council of Canada.

References

[1] Hartmann JM, Levi Di Leon R, Taine J. Line-by-line and narrow-band statistical model calculation for H_2O. J Quant Spect Radiative Transfer 1984;32(2):119–27.
[2] Soufiani A, Hartmann JM, Taine J. Validity of band-model calculations for CO_2 and H_2O applied to properties and conductive-radiative transfer. J Quant Spect Radiat Transfer 1985;33(3):243–57.
[3] Modest MF. The weighted-sum-of-gray-gases model for arbitrary solution methods in radiative transfer. ASME J Heat Transfer 1991;113:650–6.
[4] Denison MK, Webb BW. A spectral line-based weighted-sum-of-gray-gases model for arbitrary RTE solvers. ASME J Heat Transfer 1993;115:1004–11.
[5] Edwards DK. Molecular gas band radiation. In: Advances in Heat Transfer 1976;12:115–93.
[6] Lallemant N, Weber R. A computationally efficient procedure for calculating gas radiative properties using the exponential wide band model. Int J Heat Mass Transfer 1996;39:3273–86.
[7] Zhang L, Soufiani A, Taine J. Spectral correlated and non-correlated radiative transfer in a finite axisymmetric system containing an absorbing and emitting real gas–particle mixture. Int J Heat Mass Transfer 1985;31:2261–72.
[8] Kim T-K, Menart JA, Lee HS. Nongray radiative gas analysis using the S–N discrete ordinates method. ASME J Heat Transfer 1991;113:946–52.
[9] Adams BR, Smith PJ. Three-dimensional discrete-ordinates modeling of radiative transfer in a geometrically complex furnace. Combust Sci Tech 1993;88:293–308.
[10] Soufiani A, Djavdan E. A comparison between weighted sum of gray gases and statistical narrow-band radiation models for combustion applications. Combustion and Flame 1994;97:240–50.
[11] Bindar Y. Experimental and numerical investigations of a multiburner furnace operated with various heat transfer boundary conditions. Ph.D. thesis, Queen's University, Canada, 1996.
[12] Lallemant N, Weber R. Radiative property models for computing non-sooty natural gas flames. IFRF Doc No G 08/y/2, 1993.
[13] Hottel HC, Sarofim AF. Radiative Transfer. McGraw-Hill, 1967.
[14] Modak AT. Radiation from products of combustion. Fire Research 1978/1979;1:339–61.
[15] Smith TF, Shen ZF, Friedman JN. Evaluation of coefficients for the weighted sum of gray gases model. ASME J Heat Transfer 1982;104:602–8.
[16] CAGCT, CAGCT Research furnace: basic specifications and design drawings. CAGCT Technical Report, TR.96.5, 1996.
[17] Truelove JS. A mixed grey gas model for flame radiation. United Kingdom Atomic Energy Authority Report AERE-R-8494, Harwell, 1976.
[18] Rhine JM, Tucker RJ. Modelling of Gas-Fired Furnaces and Boilers. McGraw-Hill, 1991. pp. 207–8.
[19] Becker HA. Equations basic to WSGG/DOM method for chemically homogeneous gas and grey Lambert surfaces. CAGCT Memorandum, Queen's University, 1994.
[20] Carlson BG, Lathrop KD. Transport theory—the method of discrete ordinates. In: Greenspan H, Keller CN, Okrent D., editors. Computing Method in Reactor Physics. New York: Gordon and Breach, 1968.
[21] Lathrop KD. Spatial differencing of the transport equation: positivity vs. accuracy. J Computational Phys 1969;4:475–98.
[22] Thurgood CP, Becker HA, Pollard A. The T_N quadrature set for the discrete ordinates method. ASME J Heat Transfer 1995;117:1068–70.
[23] Becker HA. Representation of burner exit conditions in the mathematical modelling of large complex furnaces. In 1993 Spring Technical Meeting of the Combustion Institute Canadian Section, 1993.